First principles determination of dislocations properties of MgSiO perovskite at 30 GPa based on the Peierls-Nabarro model

Denise Ferré, Philippe Carrez, Patrick Cordier

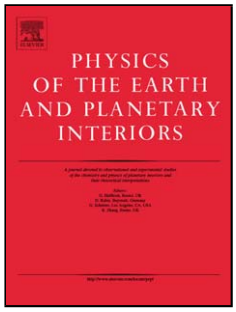

Title: First principles determination of dislocations properties of $MgSiO_3$ perovskite at 30 GPa based on the Peierls-Nabarro model

Authors: Denise Ferré, Philippe Carrez, Patrick Cordier

PII: S0031-9201(07)00122-7
DOI: doi:10.1016/j.pepi.2007.05.011
Reference: PEPI 4839

To appear in: *Physics of the Earth and Planetary Interiors*

Received date: 1-2-2007
Revised date: 20-5-2007
Accepted date: 29-5-2007

Please cite this article as: Ferré, D., Carrez, P., Cordier, P., First principles determination of dislocations properties of $MgSiO_3$ perovskite at 30 GPa based on the Peierls-Nabarro model, *Physics of the Earth and Planetary Interiors* (2007), doi:10.1016/j.pepi.2007.05.011

First principles determination of dislocations properties of $MgSiO_3$ perovskite at 30 GPa based on the Peierls-Nabarro model

Denise Ferré, Philippe Carrez and Patrick Cordier

Laboratoire de Structure et Propriétés de l'Etat Solide - UMR CNRS 8008
Université des Sciences et Technologies de Lille
Cite Scientifique, Bat C6
59655 Villeneuve d'Ascq, France

Revised

Physics of the Earth and Planetary Interiors, submitted

Corresponding author:
Patrick Cordier
Laboratoire de Structure et Propriétés de l'Etat Solide - UMR CNRS 8008
Université des Sciences et Technologies de Lille - Bat C6
59655 Villeneuve d'Ascq Cedex - FRANCE
Phone: (33) 03 20 43 43 41
Fax: (33) 03 20 43 65 91
E-mail: patrick.cordier@univ-lille1.fr

Manuscript prepared with Word X on Macintosh

≈4100 words

Abstract:

We present here a numerical modelling of dislocations in $MgSiO_3$ perovskite at 30 GPa. The dislocation core structures and properties are calculated through the Peierls-Nabarro model using Generalised Stacking Fault (GSF) results as an input. The GSF are determined from first-principle calculations using VASP. The dislocation properties such as planar core spreading and Peierls stresses are determined for the following slip systems: [100](010), [100](001), [010](100), [010](001), [001](100), [001](010), [001]($\bar{1}$10), [$\bar{1}$10](001) and [110]($\bar{1}$10) of the orthorhombic (Pbnm) perovskite structure.

Keywords: $MgSiO_3$ perovskite, deformation mechanisms, dislocations, slip systems, first-principle calculations, Peierls-Nabarro model

Introduction

The dynamics of the Earth is largely controlled by mantle convection which transports radiogenic and primordial heat toward the surface. The lower mantle, which extends between 670 and 2900 km depths, represents more than 80% of the volume of the Earth and 65% of its mass. It is hence a major component of the Earth's interior and its dynamics is of primary importance. Our understanding of the deep Earth has been changed when Liu (1974) obtained a perovskite-structured silicate after annealing a pyrope garnet at 27-32 GPa in a diamond anvil cell. Since that, numerous phase equilibrium studies have demonstrated that upper mantle assemblages decompose into a perovskite-dominated assemblage at pressures corresponding to depths below 670 km. $MgSiO_3$ perovskite (with some Fe and Al) is thus considered nowadays as the most important mineral for the interior of the Earth. Therefore, the rheology of silicate perovskite appears essential in understanding the dynamics of the Earth. Unfortunately, investigation of the rheology of $MgSiO_3$ perovskite is rendered difficult by the pressure required to reach its stability field and only a few studies have tackled this problem (Karato *et al.* 1990; Chen *et al.* 2002; Merkel *et al.* 2003, Cordier *et al.* 2004). Alternatively, many studies (listed below) have been devoted to the study of the mechanical properties of materials with the perovskite structure. Their goal was to infer the mechanical properties of $MgSiO_3$ perovskite from those of analogue materials based on the assumption that perovskites would form an isomechanical group as defined by Frost and Ashby (1982). Unfortunately, no clear systematics appeared in the creep properties of perovskite-structured materials (see for instance Beauchene & Poirier 1990). The rapid growth in available computing power has made possible to calculate the structure and properties of minerals under extreme conditions. However, mechanical properties are among the most complicated

issues to address given their intrinsic multiscale character. Indeed, plastic flow of solids involves the motion and interaction of a large number of crystal defects named dislocations. Today, this can be modelled at the mesoscale with the help of three-dimensional Dislocation Dynamics (DD) codes (Madec et al 2002, Bulatov et al. 2006). The resulting flow laws (representative of the single crystal) must be transferred to polycrystalline aggregates. At this scale, self-consistent or standard finite elements simulations can be used to describe stress and strain partitioning and interactions between grains. At this point, the greatest challenge is, upstream, to model the velocity of dislocations. This parameter is controlled, at the atomic scale, by the fine structure of the dislocation core (Hirth & Lothe 1982). The core region of dislocations can be obtained numerically in two ways: by direct atomic simulation of a defect-containing crystal, or by applying the Peierls-Nabarro model, treating dislocations as continuum objects. The use of direct atomic simulation is hindered by the lack of reliable interatomic potentials under extreme conditions. In what follows, we show how the Peierls-Nabarro model can be applied to $MgSiO_3$ perovskite to calculate dislocation properties, i.e. core structure and Peierls stress. In particular, we want here to highlight the role played by orthorhombic distortions on the dislocation structures in $MgSiO_3$ perovskite.

Structure and possible dislocations

The structure of $MgSiO_3$ perovskite consists of a corner-linked network of SiO_6 octahedra with Mg atoms located in a cavity formed by eight octahedra. The structure is orthorhombic (space group Pbnm) with a = 4.7754 Å, b = 4.9292 Å and c = 6.8969 Å (Horiuchi *et al.* 1987). This structure differs slightly from the ideal cubic perovskite (space group Pm3m) in that the octahedra are tilted and the Mg atoms are displaced from the centres of their sites (Figure 1). A pseudo-cubic lattice (with $a_c \approx 3.4$ Å) is often introduced as it provides a unified framework for all perovskites. In the following, the pseudo-cubic setting will be referred by the subscript "c" while no indication will be given when the actual orthorhombic symmetry will be used. Transformations from cubic to orthorhombic (Pbnm) or orthorhombic to cubic directions are given by:

$$\begin{pmatrix} u \\ v \\ w \end{pmatrix}_c = \begin{pmatrix} 1 & 1 & 0 \\ -1 & 1 & 0 \\ 0 & 0 & 2 \end{pmatrix} \begin{pmatrix} u \\ v \\ w \end{pmatrix}_o \quad \text{or} \quad \begin{pmatrix} u \\ v \\ w \end{pmatrix}_o = \begin{pmatrix} 1/2 & -1/2 & 0 \\ 1/2 & 1/2 & 0 \\ 0 & 0 & 1/2 \end{pmatrix} \begin{pmatrix} u \\ v \\ w \end{pmatrix}_c$$

Possible dislocations in the ideal cubic perovskite structure have been discussed by Poirier *et al.* (1989) based on structure considerations. Two possible slip systems were emphasized: $<100>_c \{001\}_c$ and $<1\bar{1}0>_c \{110\}_c$. Many deformation experiments and transmission electron microscopy (TEM) characterizations have been performed on perovskite-structured materials (not only cubic): $CaTiO_3$ (Doukhan & Doukhan 1986; Wright *et al.* 1992, Besson *et al.* 1996), $BaTiO_3$ (Doukhan & Doukhan 1986; Beauchesne & Poirier 1989; Lin & Lu 2002), $SrTiO_3$ (Nishigaki *et al.* 1991, Wang *et al.* 1993, Mao & Knowles 1996, Matsunaga & Saka 2000; Brunner *et al.* 2001; Gumbsch *et al.* 2001; Zhang *et al.* 2002a, b; Jia *et al.* 2005), $KTaO_3$ (Beauchene & Poirier 1990), $KNbO_3$ (Beauchene & Poirier 1990), $YAlO_3$ (Wang *et al.* 1999), $CaGeO_3$ (Wang *et al.* 1999). There seems to be a general trend that perovskites slip on $<1\bar{1}0>_c \{110\}_c$ at low temperature with an increasing activity of $<100>_c \{001\}_c$ (involving climb ?) at higher temperature. Very few deformation experiments have been performed on $MgSiO_3$ perovskite due to the high pressure required and to the low stability of the quenched material. Cordier *et al.* (2004) have used the x-ray peak broadening technique to investigate dislocations in a $MgSiO_3$ perovskite sample deformed in the multianvil apparatus at 25 GPa, 1400°C. [100](001) and [010](001) dislocations were identified which belong to the $<110>_c \{001\}_c$ family.

In this study, we have studied several potential slip systems in the orthorhombic structure of $MgSiO_3$ perovskite. They are listed in Table 1 in the orthorhombic and in the associated pseudo-cubic reference frame.

The Peierls-Nabarro model

The Peierls-Nabarro (PN) model (Peierls, 1940; Nabarro, 1947) represents a useful and efficient approach to calculate the core properties of dislocations based on the assumption of a planar core (Schoeck, 2005). It has been shown to apply to a wide range of materials (Wang, 1996; Bulatov & Kaxiras, 1997; Von Sydow *et al.*, 1999; Lu *et al.*, 2000, Lu, 2005; Miranda & Scandolo, 2005; Carrez *et al.* 2006; Carrez *et al., 2007a and 2007b*, Durinck *et al.* in press).

The PN model assumes that the misfit region of inelastic displacement is planar and restricted to the vicinity of the glide plane, whereas linear elasticity applies far from it. A dislocation corresponds to a continuous distribution of shear S(x) along the glide plane (x is the coordinate along the displacement direction of the dislocation in the glide plane). S(x)

represents the disregistry across the glide plane and the stress generated by such a displacement can be represented by a continuous distribution of infinitesimal dislocations with density $\rho(x)$ for which the total summation is equal to the Burgers vector b. The restoring force F acting between atoms on either sides of the interface is balanced by the resultant stress of the distribution leading to the Peierls Nabarro (PN) equation:

$$\frac{K}{2\pi}\int_{-\infty}^{+\infty}\frac{1}{x-x'}\frac{dS(x')}{dx'}dx' = \frac{K}{2\pi}\int_{-\infty}^{+\infty}\frac{\rho(x')}{x-x'}dx' = F(S(x)) \quad (1)$$

where K, the energy coefficient is function of the dislocation character. This coefficient is calculated within the framework of the Stroh theory (Hirth & Lothe, 1982) to take anisotropic elasticity into account. Originally, an analytical solution of the PN equation was proposed by introducing a sinusoidal restoring force. This simple case is only rarely found however giving the model little practical use. The PN approach was rejuvenated when Vitek (1968) showed that the restoring force introduced in the PN model is simply the gradient of the GSF γ:

$$\vec{F}(S) = -\overrightarrow{grad}\gamma(S) \quad (2)$$

In order to obtain the misfit energy corresponding to the Peierls dislocation and to determine the Peierls stress, the sum of the local misfit energy has to be done at the position of atomic planes parallel to the dislocation line. Indeed, the PN equation holds for an elastic continuous medium whereas S(x) can only be defined where an atomic plane is present (e.g. Hirth & Lothe, 1982, Schoeck, 1999). The misfit energy can be thus considered as the sum of misfit energies between pairs of atomic planes (e.g. Joos *et al.*, 1994, Joos & Duesbery, 1997) and can be written as

$$W(u) = \sum_{m=-\infty}^{+\infty}\gamma(S(ma'-u))\cdot a' \quad (3)$$

where *a'* is the periodicity of W, taken as the shortest distance between two equivalent atomic planes in the direction of the dislocation's displacement. The Peierls stress is then given by:

$$\sigma_P = \max\ \frac{1}{b}\frac{dW(u)}{du} \quad (4)$$

Computational techniques and results

First-principle calculation of Generalised Stacking Faults (GSF)

Calculations were performed using the *ab initio* total-energy calculation package VASP (Vienna Ab Initio Package) developed by Kresse and Hafner (Kresse & Hafner, 1993, 1994; Kresse & Furthmüller, 1996a). This code is based on the first-principles density functional theory and solves the effective one-electron Hamiltonian involving a functional of the electron density to describe the exchange-correlation potential. It gives access to the total energy of a periodic system with as a single input the atomic numbers of atoms. Computational efficiency is achieved using a plane wave basis set for the expansion of the single electron wave functions and fast numerical algorithms to perform self-consistent calculations (Kresse & Furthmüller, 1996b). Within this scheme, we used the Generalised Gradient Approximation (GGA) derived by Perdrew & Wang (1992) and ultrasoft pseudopotentials (e.g. Vanderbilt, 1990 or Kresse & Hafner, 1994). Computation convergence better than 4.10^{-5} eV/atom is achieved in all simulations by using a single energy cut-off value of 600 eV for the plane wave expansion. The first Brillouin zone is sampled using a Monkhorst-Pack grid (Monkhorst & Pack, 1976) adapted for each supercell geometry in order to achieve the full energy convergence. $MgSiO_3$ perovskite unit cell calculations were performed using a 4x4x2 grid with a convergence energy less than 0.25 meV for an external pressure of 30 GPa. The crystallographic structure of $MgSiO_3$ perovskite was optimised (full relaxation of the cell parameters and of the atomic positions within the cell) at 30 GPa and the obtained a, b and c lattice parameters are 4.64, 4.65 and 6.7 Å respectively (Pbnm space group). Relaxed unit cell structure and atomic positions are then used to determine the elastic constants of perovskite and to build GSF supercells. The elastic constants calculated in this study are presented in Table 2 and are found in agreement with previous determinations of Wentzcovitch *et al.* 1995, 1998 and Karki *et al.* 2000.

Calculating a GSF for a given slip system requires a supercell with an adapted geometry. Among the several possibilities of supercell construction (Bulatov *et al.* 2006), we have chosen to build all the supercells on a Cartesian reference frame defined by the normal to the stacking fault plane (located in the middle of the supercell) and by the shear direction. The last direction is then defined as the cross product of the two previous ones. A 6 Å thick vacuum layer is then added in the direction normal to the slip plane to avoid interaction between repeated stacking fault resulting from the use of periodic boundary conditions. The GSF excess energies γ are calculated by imposing a given shear displacement value to the upper part of the supercell. The atoms close to the shear plane are allowed to relax in order to minimize the energy of the stacking fault. This is obtained by (i) keeping the supercell vectors

fixed at the values obtained for a bulk system submitted to the pressure of interest, (ii) maintaining fixed the atoms present on the two surfaces (to mimic the action of the surrounding bulk and of pressure) and (iii) allowing relaxations of others atoms in the directions normal to the shear direction. This calculation method ensures that the relaxation scheme is equivalent for the nine GSF calculations previously cited and enables us to study the effect of octahedra distortions on the symmetry of the GSF. Finally, the Monkhorst-Pack grid is adapted to the supercell parameters. As an example, using a 6x2x4 grid for a [100](010) GSF calculation guaranties accuracy better than 0.01 %.

The GSF calculated along this procedure are presented Figure 2 for the nine slip systems considered in this study: [100](010), [100](001), [010](100), [010](001), [001](100), [001](010), [001]($\bar{1}$10), [$\bar{1}$10](001) and [110]($\bar{1}$10).

Peierls model

In this paper, we follow the methodology proposed by Joos *et al.* (1994) and already applied to Mg_2SiO_4 ringwoodite by Carrez *et al.* (2006) to determine the disregistry function S of any dislocation incorporating the results of GSF calculations. Within this approach, S(x) is obtained by searching for a solution in the form:

$$S(x) = \frac{b}{2} + \frac{b}{\pi} \sum_{i=1}^{N} \alpha_i \cdot \arctan \frac{x - x_i}{c_i} \tag{5}$$

where α_i, x_i and c_i are variational constants. Substituting this disregistry into the left-hand side of the PN equation (1), gives the restoring force

$$F^{PN}(x) = \frac{Kb}{2\pi} \sum_{i=1}^{N} \alpha_i \cdot \frac{x - x_i}{(x - x_i)^2 + c_i^2} \tag{6}$$

The variational constants α_i, x_i and c_i are obtained from a least-square minimisation of the difference between F^{PN} and the restoring force F calculated from first-principles calculations. Practically, the order N of decomposition series is adjusted (usually between 3 and 6) to the complexity (symmetry, number of maxima) of the restoring force curves as determined after first-principles calculations. For each slip system, we present on Figure 3, the screw dislocation core disregistry S and the dislocation core densities ρ (=dS/dx) as a function of the distance x to the dislocation core centre.

From the PN model to a representation of the dislocation core

The shear profile *S(x)* across the dislocation core is given by the PN model. It can be used to build an atomistic model of the dislocation core. We start from a perfect crystal. Following the Peierls approach, the crystal is split into two parts above and below the glide plane. The dislocation is introduced by firstly shifting the initial upper part by a value of b/2. The extension of the core (as determined by the Peierls-Nabarro method presented in the previous section) is then imposed by adjusting all the atomic positions according to the shear profile *S(x)* calculated in the PN model. As a consequence, the upper part of the crystal is stretched whereas the lower part is compressed and a crystal with a dislocation in the centre is formed (details of the construction can be found in Hirth & Lothe 1982 or in Wang 1996). At this stage, the elastic displacement field associated with the dislocation density ρ (the equation can be found in Carrez *et al.* 2007a) is added at any atomic position, which results in a reduction of the atomic plane distortions far from the dislocation centre. Typical examples of edge core structures are presented on figure 4.

Discussion

Plastic deformation of $MgSiO_3$ perovskite: cubic or orthorhombic ?

One of the first motivations of this work was to assess the influence of the orthorhombic distortions on the plastic properties of $MgSiO_3$ perovskite. This influence can be readily judged from the visual aspects of the GSF (Figure 2). With the exception of slip systems involving the [001] direction, all GSF are asymmetric. This is the result of the octahedra being tilted in the orthorhombic structure. Another consequence of the orthorhombic distortions is that some Burgers vectors are twice as large as in the cubic perovskite: for instance [110], $[\bar{1}10]$ and [001] which correspond respectively to $2\times[100]_c$, $2\times[010]_c$ and $2\times[001]_c$. It was expected that this situation would lead to dislocations dissociated into two partials with collinear Burgers vectors (Poirier *et al.* 1989). Indeed, we find that these slip systems are characterized by camel-hump GSF (Figure 2) which lead to dislocations being split into two collinear partials (Figure 3 and Figure 4b). The stacking fault energy at the minimum of the GSF (half-shear) is thus a direct assessment of the distortions as this value would be zero in the cubic structure. One can see on Figure 2 that the orthorhombic distortions of $MgSiO_3$ perovskite cannot be neglected. A direct consequence of these relatively high values of the stacking fault energies is that the separation distance between partial dislocations is rather small: 15-25 Å (Table 3). One can also directly compare slip systems that would be equivalent in an ideal, undistorted, perovskite structure, for instance $[100](010)$ and

[010](100) (i.e. $[1\bar{1}0]_c(110)_c$ and $[110]_c(1\bar{1}0)_c$, see Table 1 and Figures 2a and 2c), [100](001) and [010](001) ($[1\bar{1}0]_c(001)_c$ and $[110]_c(001)_c$, see Figures 2b and 2d), [001](100) and [001](010) ($[001]_c(1\bar{1}0)_c$ and $[001]_c(110)_c$, see Figures 2e and 2f) or [001]($\bar{1}$10), [$\bar{1}$10](001) and [110]($\bar{1}$10) ($[001]_c(010)_c$,$[010]_c(001)_c$ and $[100]_c(010)_c$ respectively, see Figures 2g, 2h and 2i). The differences can be appraised from the aspect of the GSF, or more quantitatively from the Peierls stresses which can be in some cases significantly different (see for instance [100](001) for which the Peierls stresses are almost twice as large as those of [010](001)). All together, these observations show that the orthorhombic distortions of the $MgSiO_3$ perovskite play an important role on the dislocation structures and properties. The orthorhombic lattice appears to be the only relevant framework to describe the plastic properties of $MgSiO_3$ perovskite. One can thus question the relevance of the use of analogue materials (with distinct space groups and distortions) in the study of plastic deformation of perovskites. Indeed, several authors have noticed significant discrepancies among so-called analogues (Poirier *et al.* 1989, Beauchesne & Poirier 1990, Wright *et al.* 1992, Wang *et al.* 1993, Wang *et al.* 1999). It appears necessary to investigate the dislocation properties of perovskites with different structures in order to assess if some common features can be found and can be used within the framework of an isomechanical approach.

Dislocation core structures

The shortest lattice vectors in the $MgSiO_3$ perovskite structure are [100] (4.8Å) and [010] (4.9Å). The corresponding dislocations appear to have relatively narrow cores (Figures 3a-d): of the order of 2-4Å for screw dislocations. Edge dislocations exhibit wider dislocation cores. This is a general fact due to the introduction of the Poisson ratio in the relations of edge dislocations (Hirth & Lothe 1982). Although that is not readily seen on atomic models, the influence of orthorhombic distortions can be found in the fine core structure of dislocations. Only [100] dislocations gliding in (001) exhibit a single-peaked dislocation profile. The core profile of [100](010) and [010] dislocations could be described as the sum of two, strongly overlapping, partial dislocations. These partials are sometimes unlike, leading to an asymmetric profile of the dislocation core. As noticed above, orthorhombic distortions imply that some Burgers vectors are twice as large as in the cubic perovskite. The next Burgers vectors are then [001], [$\bar{1}$10] and [110] with magnitudes close to 6.9 Å. All these dislocations exhibit very comparable core structure with narrow (half-widths of the order of 1-1.5 Å) collinear partials separated by a distance of the order of 15-25 Å.

Peierls stresses

One of the merits of the PN model is, beyond the description of the core, to provide mechanical data in the form of the stress necessary to move a straight dislocation at 0K over the Peierls barrier, the so-called Peierls stress (equation 4). The values of Peierls stresses depend on the character of the dislocation line. They are given for edge and screw dislocations in Table 3. Edge and screw dislocations do not generally exhibit the same Peierls friction and this is observed with $MgSiO_3$ perovskite. However, we see that Peierls friction for edge and screw dislocations stay generally within a factor of two. It is not expected thus that edge and screw segments will exhibit very different mobilities and dislocation loops are likely to expend quasi-isotropically. Among the slip systems investigated, two appear to be easier to activate: [100](010) and [010](100). On the opposite side, [001](100) and [001](010) appear to be the hardest slip systems (remembering that the harder character is likely to control the activity of a given slip system). In between, the difference in Peierls friction is not large enough to exclude any slip system *a priori*. In particular, one finds here the two slip systems identified by Cordier *et al.* (2004) in experimentally deformed $MgSiO_3$ perovskite. It is interesting to note that the magnitude of the Burgers vector is not enough to constrain the mechanical properties as, for instance, [100](001) and [001]($\bar{1}$10) or [$\bar{1}$10](001) exhibit very similar Peierls stresses despite significantly different Burgers vectors. This is probably due in part to the fact that dislocations with larger Burgers vectors are dissociated, a factor which is known to enhance dislocation mobility.

Let us compare Peierls stresses in $MgSiO_3$ perovskite with other silicates. Carrez *et al.* (2006) have calculated the Peierls stresses in Mg_2SiO_4 ringwoodite at 20 GPa following the same procedure as the present one. The Peierls stresses for ½<110> screw dislocations in Mg_2SiO_4 ringwoodite lie in the range 10-34 GPa. We don't observe a strong contrast between the intrinsic resistances to plastic shear of these two silicates although the shear mechanisms are markedly different. Mg_2SiO_4 ringwoodite, is a silicate based on SiO_4 tetrahedra for which plastic shear can be achieved without shearing the strong tetrahedral units (and hence the Si-O bonds). The situation is very different with $MgSiO_3$ perovskite as all slip system involve shearing the Si-O bonds of the SiO_6 octahedra. It must be remembered however that Si-O bonds are longer, and hence weaker, in octahedra than in tetrahedra. Together with the ability of some dislocations to dissociate in $MgSiO_3$ perovskite, that might explain the relatively modest strength contrast between Mg_2SiO_4 ringwoodite at 20 GPa and $MgSiO_3$ perovskite at 30 GPa. A more wide comparison can be done by normalizing mechanical data. This is usually achieved by dividing stress (here the Peierls stress) by an appropriate modulus (Frost and Ashby 1982). We use the shear modulus $\mu_{[uvw](hkl)}$ calculated in anisotropic elasticity for

each slip system. Using this approach, we find that the Peierls stresses fall in the range 0.04-0.19 for screw dislocations and 0.04-0.29 for edge dislocations. This is very comparable with values previously calculated for other silicates: forsterite (0.08-0.4 for [100] dislocations and 0.02-0.09 for [001] dislocations, see Durinck *et al.* in press), ringwoodite (0.01-0.2 from Carrez *et al.* 2006) and $MgSiO_3$ post-perovskite (0.001-0.01, see Carrez *et al.* 2007b). In particular, we don't observe any drastic difference in mechanical properties between tetrahedra- and octahedra-based silicates.

Concluding remarks

We have used the Peierls-Nabarro approach to propose the first model of dislocation core structures in orthorhombic $MgSiO_3$ perovskite calculated at 30 GPa.

- We show that the orthorhombic distortions have a significant influence on the dislocation core fine structure as well as on the Peierls friction. Hence (and contrary to what was implicitly assumed in Cordier *et al.* 2004), the plasticity of $MgSiO_3$ perovskite must be described within the frame of orthorhombic symmetry only.
- Most dislocations exhibit a tendency for core spreading ([100](001) is the only exception). This tendency is strongly controlled by the orthorhombic distortions (octahedral tilting). Only [001], $[\bar{1}10]$ and [110] show clear dissociation into well-defined partial dislocations. Following the example of bcc metals and [001] dislocations in forsterite, this ability of [001] dislocations to spread into several planes raises the question of a possible three-dimensional core. This issue which shows the limits of the present modelling has profound implications on dislocation mobilities and calls for further studies.
- The difference in mobility between slip systems (inferred here from the Peierls friction) is not so marked that some slip systems can be excluded a priori in further modelling of $MgSiO_3$ perovskite plasticity.
- The present study casts some light on the observation that perovskites do not constitute an isomechanical group. This approach should be extended to other perovskite-structured materials to better highlights the differences and possible similarities between these materials.

References:

Beauchesne, S. and Poirier, J. P., 1989, *Phys. Earth Planet. Int.*, **55**, 187.

Beauchesne, S. and Poirier, J. P., 1990, *Phys. Earth Planet. Int.*, **61**, 182.

Besson, P., Poirier, J. P. and Price, G. D., 1996, *Phys. Chem. Minerals*, **23**, 337.

Brunner, D., Taeri-Baghbadrani, S., Sigle, W. and Rühle, M., 2001, *J. Am. Ceram. Soc.*, **84**, 1161.

Bulatov, V. V., Cai, W., Baran, R. and Kang, K., 2006, *Phil Mag*, **86**, 2847.

Bulatov, V. V. and Kaxiras, E., 1997, *Phys. Rev. Lett.*, **78**, 4221.

Carrez, P., Cordier, P., Mainprice, D. and Tommasi, A., 2006, *Eur. J. Mineral.*, **18**, 149.

Carrez, P., Ferré, D. and Cordier, P., 2007a, Nature, 446, 68

Carrez, P., Ferré, D. and Cordier, P., 2007b, *Phil Mag*., DOI 10.1080/14786430701268914

Chen, J. H., Weidner, D. J. and Vaughan, M. T., 2002, *Nature*, **419**, 824.

Cordier, P., Barbe, F., Durinck, J., Tommasi, A. and Walker, A. M. 2005. Plastic deformation of minerals at high pressure: multiscale numerical modelling. In: *Mineral behaviour at extreme conditions* (edited by Miletich, R.). *EMU Notes in Mineralogy* **7**. Eötvös University Press, Budapest, 389.

Cordier, P., Ungár, T., Zsoldos, L. and Tichy, G., 2004, *Nature*, **428**, 837.

Doukhan, N. and Doukhan, J. C., 1986, *Phys. Chem. Minerals*, **13**, 403.

Durinck, J., Carrez, P. and Cordier, P., (in press), *Eur. J. Mineral.*

Frost, H. J. and Ashby, M. F., 1982, *Deformation-mechanism maps*.(Oxford: Pergamon Press). p.166.

Gumbsch, P., Taeri-Baghbadrani, S., Brunner, D., Sigle, W. and Rühle, M., 2001, *Phys. Rev. Lett.*, **87**.

Hirth, J. P. and Lothe, J., 1982, *Theory of dislocations*.(New York: John Wiley & Sons, Inc).

Horiuchi, H., Ito, E. and Weidner, D. J., 1987, *Am. Mineral.*, **72**, 357.

Jia, C. L., Thust, A. and Urban, K., 2005, *Phys. Rev. Lett.*, **95**, 225506.

Joos, B. and Duesbery, M. S., 1997, *Phys. Rev. Lett.*, **78**, 266.

Joos, B., Ren, Q. and Duesbery, M. S., 1994, *Phys. Rev. B*, **50**, 5890.

Karato, S. I., 1990, *Geophys. Res. Lett.*, **17**, 13.

Karki, B. B., Wentzcovitch, R. M., de Gironcoli, S. and Baroni, S., 2000, *Phys. Rev. B*, **62**, 14750.

Kresse, G. and Furthmüller, J., 1996a, *Phys. Rev. B*, **54**, 11169.

Kresse, G. and Furthmüller, J., 1996b, *Comput. Mat. Sci.*, **6**, 15.

Kresse, G. and Hafner, J., 1993, *Phys. Rev. B*, **47**, 558.

Kresse, G. and Hafner, J., 1994, *Phys. Rev. B*, **49**, 14251.

Lin, M.-H. and Lu, H.-Y., 2002, *Mater Sci Eng A-Struct Mater*, **A333**, 41.

Liu, L., 1974, *Geophys. Res. Lett.*, **1**, 277.

Lu, G. 2005. The Peierls-Nabarro Model of Dislocations: A venerable theory and its current development. In: *Handbook of Materials Modeling. Volume 1: Methods and Models* (edited by Yip, S.). Springer, 1.

Lu, G., Kioussis, N., Bulatov, V. V. and Kaxiras, E., 2000, *Phys. Rev. B*, **62**, 3099.

Mao, Z. and Knowles, K. M., 1996, *Phil Mag A*, **73**, 699.

Matsunaga, T. and Saka, H., 2000, *Phil Mag Letters*, **80**, 597.

Merkel, S., Wenk, H. R., Badro, J., Montagnac, G., Gillet, P., Mao, H. K. and Hemley, R. J., 2003, *Earth Planet Sci Lett*, **209**, 351.

Miranda, C. R. and Scandolo, S., 2005, *Comp. Phys. Comm.*, **169**, 24.

Monkhorst, H. J. and Pack, J. D., 1976, *Phys. Rev. B*, **23**, 5048.

Nabarro, F. R. N., 1947, *Proc. Phys. Soc. Lond.*, **59**, 256.

Nishigaki, J., Kuroda, K. and Saka, H., 1991, *Phys. Stat. Sol. (a)*, **128**, 319.

Peierls, R. E., 1940, *Proc. Phys. Soc. Lond.*, **52**, 34.

Perdew, J. P. and Wang, Y., 1992, *Phys. Rev. B*, **45**, 13244.

Poirier, J. P., Beauchesne, S. and Guyot, F. 1989. Deformation mechanisms of crystals with perovskite structure. In: *Perovskite: a structure of great interest to geophysics and materials science* (edited by Navrotsky, A. & Weidner, D.). AGU, Washington DC, 119.

Schoeck, G., 1999, *Philos. Mag. A*, **79**, 2629.

Schoeck, G., 2005, *Mater. Sci. Eng. A*, **400-401**, 7.

Vanderbilt, D., 1990, *Phys. Rev. B*, **41**, 7892.

Vítek, V., 1968, *Phil. Mag.*, **18**, 773.

von Sydow, B., Hartford, J. and Wahnström, G., 1999, *Comp. Mat. Sci.*, **15**, 367.

Wang, J. N., 1996, *Mater. Sci. Eng. A*, **206**, 259.

Wang, Z. C., DupasBruzek, C. and Karato, S., 1999, *Phys Earth Planet Interiors*, **110**, 51.

Wang, Z. C., Karato, S. and Fujino, K., 1993, *Phys Earth Planet Interiors*, **79**, 299.

Wentzcovitch, R. M., Karki, B. B., Karato, S. and DaSilva, C. R. S., 1998, *Earth Planet Sci Lett*, **164**, 371.

Wright, K., Price, G. D. and Poirier, J. P., 1992, *Phys. Earth Planet. Int.*, **74**, 9.

Zhang, Z., Sigle, W., Kurtz, W. and Rühle, M., 2002, *Phys. Rev. B*, **66**, 214112.

Zhang, Z., Sigle, W. and Rühle, M., 2002, *Phys. Rev. B*, **66**, 094108.

Orthorhombic	*Cubic*
[100](010)	$[1\bar{1}0]_c(110)_c$
[100](001)	$[1\bar{1}0]_c(001)_c$
[010](100)	$[110]_c(1\bar{1}0)_c$
[010](001)	$[110]_c(001)_c$
[001](100)	$[001]_c(1\bar{1}0)_c$
[001](010)	$[001]_c(110)_c$
[001]($\bar{1}$10)	$[001]_c(010)_c$
[$\bar{1}$10](001)	$[010]_c(001)_c$
[110]($\bar{1}$10)	$[100]_c(010)_c$

Table 1*: Slip systems investigated in the present study indexed in the orthorhombic (Pbnm) and pseudo-cubic settings.*

C_{11}	C_{22}	C_{33}	C_{44}	C_{55}	C_{66}	C_{12}	C_{13}	C_{23}
592	672	617	235	203	192	214	197	216

Table 2*: Elastic constants (in GPa) of $MgSiO_3$ perovskite calculated at 30 GPain this study.*

Slip system	ISS (GPa)	Screw dislocations			Edge dislocations		
		σ_P (GPa)	ξ (Å)	Δ (Å)	σ_P (GPa)	ξ (Å)	Δ (Å)
[$\bar{1}$00](010)	43.2	15.5	3	-	7	4.3	-
[100](001)	62.7	39	1.8	-	18	2.5	-
[010](100)	40.9	8	4	-	7	5.3	-
[010](001)	59.4	22.5	2.4	-	10	3.5	-
[001](100)	82.1	23	1	13.1	58	1.3	16.4
[001](010)	74.4	44	0.95	15.3	67.5	1.25	20.4
[001]($\bar{1}$10)	61.2	39.5	1.3	19.2	20	1.7	24
[$\bar{1}$10](001)	56.7	34	1.4	12.7	17	1.9	16.5
[110]($\bar{1}$10)	61.2	33.5	1.3	12	36	1.6	15

***Table 3**:* Ideal shear stress (ISS defined as the maximum of the restoring force F) and dislocation properties at P = 30 GPa. σ_p is the Peierls stress, ξ is the half-width of the dislocation (or partial) distribution and Δ is the partial separation (only given when partials are well-defined).

Figures

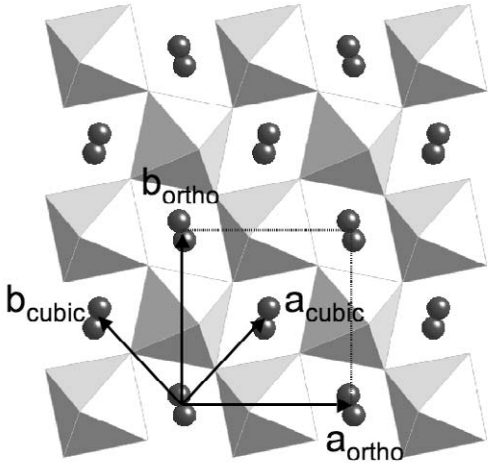

Figure 1*: Structure of the orthorhombic, $MgSiO_3$ perovskite viewed down [001]. The Pbnm orthorhombic unit cell is represented together with the pseudo-cubic lattice vectors as defined in the text. Note that* $c_{ortho} = 2c_{cubic}$.

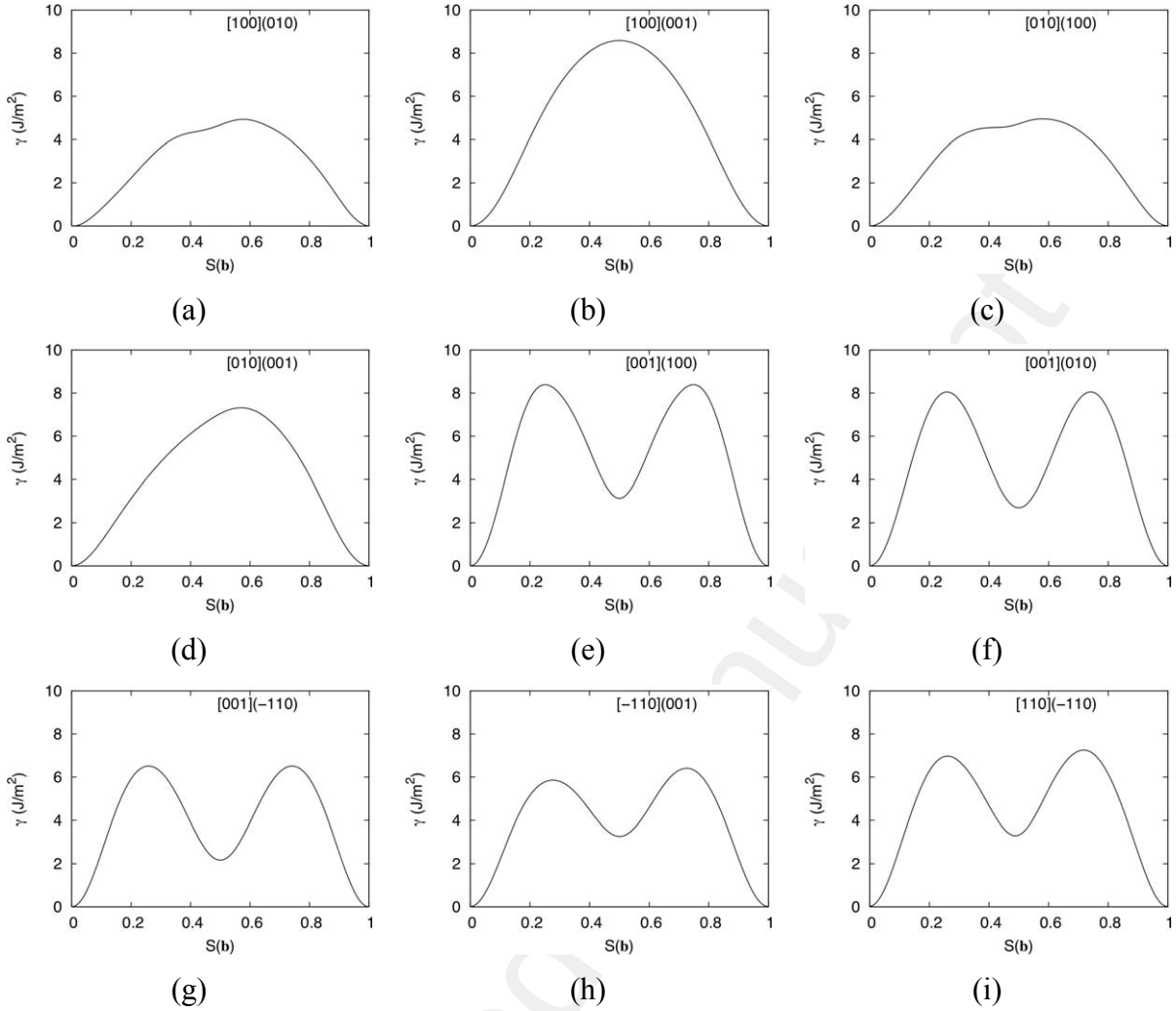

***Figure 2**: GSF calculated in $MgSiO_3$ perovskite at 30 GPa for the following slip systems*:

a) [100](010) - *b)* [100](001) - *c)* [010](100) - *d)* [010](001) - *e)* [001](100)

f) [001](010) - *g)* [001]($\bar{1}$10) - *h)* [$\bar{1}$10](001) - *i)* [110]($\bar{1}$10)

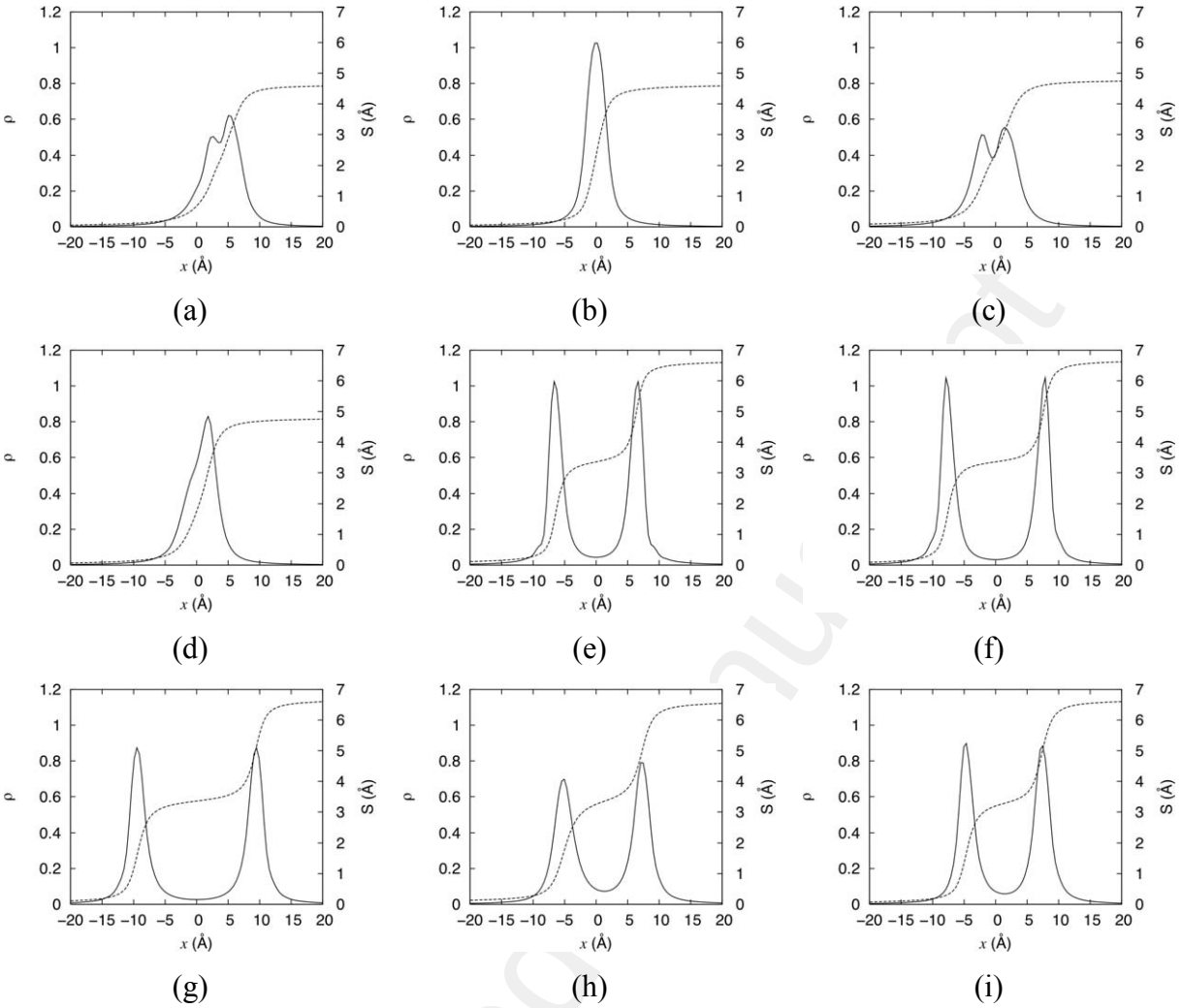

***Figure 3**: Dislocation density ρ (solid line) and disregistry (dotted line) for screw dislocations in $MgSiO_3$ perovskite calculated at 30 GPa for the following slip systems:*
a) [100](010) - *b)* [100](001) - *c)* [010](100) - *d)* [010](001) - *e)* [001](100)
f) [001](010) - *g)* [001]($\bar{1}$10) - *h)* [$\bar{1}$10](001) - *i)* [110]($\bar{1}$10)

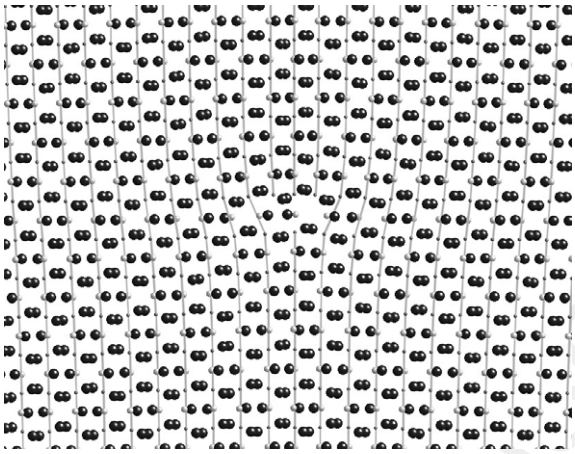

a)

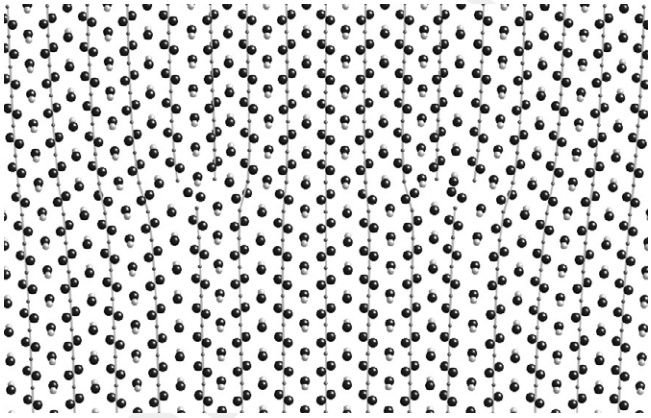

b)

Figure 4*: Atomic model of two dislocation cores. Silicon lattice planes are highlighted for an easier recognition of the dislocation. Small grey spheres, light grey spheres and black spheres correspond respectively to silicon, magnesium and oxygene atoms.*

a) [100](001) *dislocation. The structure is viewed down [010]*

b) [001](010) *dislocation. The structure is viewed down [100]*